Fabrication of heterojunction crystalline Si solar cells with $BaSi_2$ thin films prepared by 2-step evaporation method

Yoshihiko Nakagawa[1]*, Kazuma Takahashi[1], Michinobu Fujiwara[1], Kosuke O. Hara[2], Kazuhiro Gotoh[1], Yasuyoshi Kurokawa[1], Takashi Itoh[1], Takashi Suemasu[3], and Noritaka Usami[1]

[1] *Department of Materials Process Engineering, Nagoya University, Nagoya 464-8603, Japan*

[2] *Center for Crystal Science and Technology, University of Yamanashi, Kofu 400-8511, Japan*

[3] *Graduate School of Engineering, Tsukuba University, Tsukuba 305-8573, Japan*

*E-mail: yoshihiko.nakagawa@usa-labo.nagoya

We have fabricated p-type $BaSi_2$ (p-$BaSi_2$)/n-type crystalline Si (n-c-Si) heterojunction solar cells using thermal evaporation. To control the defect around the heterointerface, samples were fabricated by two methods using different current profiles during evaporation. One-step method was designed to avoid supplying Ba-rich vapor, and two-step method was designed to intentionally introduce Ba-rich vapor at the first step. Deep-level transient spectroscopy measurements revealed that defect densities in n-c-Si side were almost the same for both samples. Open-circuit voltage (V_{oc}) was successfully improved from 319 to 463 mV by the two-step method. This may be due to the increase of carrier density in p-$BaSi_2$ prepared using two-step method. As a result of optimization, the conversion efficiency of 6.23% was achieved by the heterojunction solar cells.

1. Introduction

To realize solar cells with high conversion efficiency at low cost, numerous researchers have pursued alternative materials to Si such as perovskite, Cu(In,Ga)Se, CdTe and so on [1-3]. As one of the promising materials, we have investigated $BaSi_2$ with prominent suitable-characteristics for solar cells. $BaSi_2$ consists of abundant elements of Ba and Si, and exhibits n-type conductivity in non-doped state if one does not precisely control the flux ratio [4-6]. The bandgap is ~1.3 eV [4,7], which is close to ideal value of 1.4 eV for single junction solar cells, and the electron affinity is 3.2 eV [8]. Several prominent characteristics have been found including the minority carrier lifetime τ=10 μs [9-11], minority carrier diffusion length L~10 μm [12,13] and absorption coefficient 3.0×10^4 cm^{-1} at photon energy of 1.5 eV [14-16]. Accordingly, the materials have attracted attention as absorption layer alternative to crystalline Si (c-Si). In fact, the $BaSi_2$ pn junction solar cells are expected to achieve conversion efficiency of 25% with only thickness of 2 μm [17]. As a simple method to prepare $BaSi_2$ films, we have utilized thermal evaporation using $BaSi_2$ compound as a source, and revealed the growth mechanism and characteristics of the $BaSi_2$ films [18-24]. As a result, the films demonstrated a long carrier lifetime of 27 μs [25] and the photoresponse property [26], indicating that $BaSi_2$ films prepared by thermal evaporation are promising for solar cells.

We recently have proposed to adopt p-type $BaSi_2$ (p-$BaSi_2$) to hole selective material as one of the promising applications of $BaSi_2$. In theory, minority holes generated in n-type c-Si (n-c-Si) can be transmitted through p-$BaSi_2$/n-c-Si interface, while majority electrons are repelled there due to high conduction band offset [27]. The conversion efficiency of 9 % has been reported for the p-$BaSi_2$/n-c-Si heterojunction solar cells using the p-$BaSi_2$ thin films prepared by molecular beam epitaxy (MBE) method [28, 29]. Based on the accumulated knowledge of the $BaSi_2$ evaporation, we developed the new fabrication method, which consists of thermal evaporation of $BaSi_2$ on B-doped hydrogenated amorphous Si (a-Si:H) deposited by plasma enhanced chemical vapor deposition (PECVD) [30]. This method permitted the preparation of B-doped p-$BaSi_2$ on a large area Si substrate. The hole density and carrier mobility obtained from the films were 7.3×10^{19} cm^{-3}, and 3.8 $cm^2/V \cdot s$, respectively, which are sufficient values to reach high open-circuit voltage (V_{oc}) for p-$BaSi_2$/n-c-Si heterojunction solar cells. In order to apply the p-$BaSi_2$ films to p-$BaSi_2$/n-c-Si

heterojunction solar cells, the control of the interface is of crucial importance. Especially, the deposition control of initial stage of source heating would give large impact on the interface between p-$BaSi_2$ and n-c-Si owing to the initial Ba-rich vapor [24].

In this study, we report the fabrication of p-$BaSi_2$/n-c-Si heterojunction solar cells by using thermal evaporation with different two methods to reduce defects around pn interface. The first method is designed to prevent extra Ba from diffusing into n-c-Si by heating the source material at high temperature. The second method is designed to form stoichiometric p-$BaSi_2$ by reaction of Ba with p-type a-Si:H at the first step, and grow the rest of $BaSi_2$ layer on that at the second step. Structural and electrical properties of $BaSi_2$ films and solar cells prepared by both methods are compared. Finally, the structure and current density (*J*)-voltage (*V*) characteristics of solar cells using an optimized source heating method are demonstrated.

2. Experimental method

B-doped a-Si:H thin films with about thickness of 10 nm were deposited on n-c-Si(111) substrate (resistivity=1-4 Ω·cm and area=1.44 cm^2) by PECVD. Substrate temperature was kept at 180 °C during the deposition. The gas flow rates of SiH_4, H_2, and 1% B_2H_6 were same and set at 40 sccm. The B concentration in the p-type a-Si:H was 20 times higher than as evidenced by the hole density of 1.8×10^{20} cm^{-3} obtained from the same sample after crystallization. The $BaSi_2$ was prepared on the B-doped a-Si:H by thermal evaporation. We used $BaSi_2$ granules (99 % in purity, Kojundo Chemical, Ltd.) as a source material for thermal evaporation. The granules were placed on a tungsten boat in an evaporation chamber. The granules were melted using resistive heating of the boat. According to our previous study, the weight of $BaSi_2$ was chosen as 0.015 g since extra Ba could be consumed completely by the a-Si:H layer. Two different heating current profiles were used as shown in Fig. 1. One is the same method as the previous study (hereafter, this sample is called “one-step”). The temperature on the boat was gradually increased by controlling the current from 0 to 50 A until 300 s. After that, the current was increased and kept at 80 A around 10 s. Subsequently, shutter was opened to start the deposition at 310 s and current density was increased at 140 A. Finally, the deposition was finished at 360 s. This method aims to prevent excess Ba from diffusing to n-c-Si side and to reduce the defect derived from Ba in n-c-Si around the

heterointerface. On the other hand, in the case of the second method, after the source material was melted at a lower temperature, the temperature on the boat was increased (hereafter, this sample is called "two-step"). Before the first step, the current was increased to 50 A until 300 s. After opening the shutter, the current was increased to 90 A and kept for 20 s (The first step). After that, the current was increased from 90 to 140 A for 10 s and kept for 30 s (The second step). This method aims to prepare stoichiometric p-$BaSi_2$ to reduce defects on the p-$BaSi_2$ film side at the pn-interface. During this evaporation, substrate temperature was kept at 600 °C. After the evaporation, the samples were annealed at 700 °C for 10 min under Ar flow (purity: 99.9999%). The prepared thin films were analyzed by Raman scattering spectroscopy (Tokyo Instruments Nanofinder) with an Ar^+ ion laser (λ= 488 nm). For electrical measurement, Au-Ga ohmic contacts were formed on the surface of the films and Au-Sb ohmic contacts were formed on the back side of the sample by thermal evaporation, respectively. The depth profiles of Ba and Si were obtained from Auger electron spectroscopy (AES). The deep-level transient spectroscopy (DLTS) measurement was performed in the temperature range between 70–300 K. Pulse width, forward voltage, and reverse voltage are 50 ms, +0.5 V, and -0.1 V, respectively. Finally, from above these results, we attempted to optimize the solar cell structures by employing $BaSi_2$ prepared by the two-step method and back surface field layer (n^{++}-Si layer) to achieve high conversation efficiency. In order to increase short-circuit current density (J_{sc}), the film thickness of p-$BaSi_2$ layer was reduced to 25 nm. In addition, 80-nm-thick indium tin oxide (ITO) layer was deposited onto p-$BaSi_2$ by Radio frequency (RF)-sputtering for anti-reflection coating. Ag finger electrodes were deposited onto the ITO layer by thermal evaporation. *J-V* measurement was carried out under the solar simulator illumination at AM1.5G, 100 mW/cm^2, and room temperature.

3. Results and discussion

A schematic of the p-$BaSi_2$/n-c-Si heterojunction solar cells is shown in Fig. 2(a). Light and dark *J-V* curves for three cells fabricated with either the one-step or two-step process can be seen in Figs. 2(b) and 2(c), respectively. V_{oc}, J_{sc}, fill factor (*FF*), and conversion efficiency (η) are shown in Table I. Both of the cells showed rectifying characteristics, suggesting that pn junctions were successfully formed. From the dark *J-V* curves, the one-step and two-step

samples show the current density is saturated in the voltage range over 200, and 500 mV, respectively. This result suggests that a blocking layer against majority carriers was formed in the solar cells. This saturation of current density could be attributed to the formation of oxide layers on the surface of p-$BaSi_2$ layer or heterointerface of p-$BaSi_2$/n-c-Si. According to a previous report, oxides exist at the $BaSi_2$/Si heterointerface since Si surface was oxidized or initial Ba-rich layer was oxidized [31]. Note that this layer is not necessarily uniform. One candidate of oxides is BaO since $BaSi_2$ reacts with trace amount of oxygen above 600 °C as reported before [32]. If the BaO layer was formed around heterointerface, band diagram is calculated as Fig. 2(d). The band diagram was calculated by a one-dimensional device simulator, Afors-HET ver 2.5 [33]. Since electron affinity of BaO is 0.57 eV [34], this layer could be a blocking layer for electron.

Compared to the one-step sample, V_{oc}, J_{sc} and FF of the two-step sample were improved. Especially, V_{oc} was significantly improved by 45%. The J-V characteristics can be written using the series resistance (R_s) and the shunt resistance (R_{sh}) as the following equation (1).

$$J = J_0\left[\exp\left\{\frac{q\left(V+R_sJ\right)}{nk_BT}\right\}-1\right]+\frac{V+R_sJ}{R_{sh}} \qquad (1)$$

Here, J_0 is saturation current density, q is elementary charge, n is ideal factor, T is temperature, and k_B is Boltzmann constant. By fitting the obtained J-V characteristics with the Eq. (1), R_{sh} of the one-step and two-step samples were estimated at 2.94, and 4.56 Ω·cm^2, respectively. It is considered that FF of the one-step sample is smaller than that of the two-step sample due to leakage current since R_{sh} of the one-step sample is smaller than two-step sample. In addition, J_0 of the one-step and two-step samples were 0.14, and 1.5×10^{-4} A/cm^2, respectively. V_{oc} can be calculated according to following equation (2).

$$V_{oc} = \frac{nk_BT}{q}\ln\left(\frac{J_{sc}}{J_0}+1\right) \qquad (2)$$

Since J_{sc} is in the same order for the both samples, J_{sc} is not responsible for the difference in V_{oc}. J_{sc} of two-step sample is slightly increased compering to the one-step sample and this

improvement of J_{sc} is caused by the decrease of R_s. R_s of the one-step sample and two-step samples are 0.414, and 0.229 Ω·cm^2, respectively. This decrease of R_s is caused by decreasing sheet resistance of p-$BaSi_2$ due to the increase of carrier density. *n* for the one-step sample is same as that of the two-step sample and the value was 1.1. From these results, we have concluded that the decrease of R_s and increase of R_{sh} lead to the increase of *FF* of the two-step sample.

Figure 3 shows Raman scattering spectra of the one-step and two-step samples. The peak around 521 cm^{-1} derived from c-Si and five peaks derived from $[Si_4]^{4-}$ in $BaSi_2$ [35] can be seen. The c-Si peak might come from Si substrate since the incident light reached the substrate through the $BaSi_2$ film with the thickness of approximately 23~30 nm. The peak of $BaSi_2$ A_g around 485 cm^{-1} [36] was fitted by the Lorentz function to obtain the full width at half maximum (FWHM). FWHM of the two-step sample was 7.44 cm^{-1} and that of the one-step sample was 7.54 cm^{-1}. This result indicates that crystal quality of the films is almost the same.

Figures 4(a) and 4(b) show depth profiles of the Ba, Si, and O atomic composition of the one-step and two-step samples measured by AES. Note that approximate 70 nm-thick ITO region exists on the front side of the sample to prevent $BaSi_2$ from the progress of oxidation due to atmosphere exposure. Judging from distribution of Ba composition profile, we can identify the surface position of p-$BaSi_2$ film and around the $BaSi_2$/n-c-Si heterointerface. The region in the depth of 70 to 100 nm is the oxide layer by taking the O composition profile into account. The film thicknesses for the one-step and two-step samples are approximately 30 and 23 nm, respectively. The oxygen profile of both samples around p-$BaSi_2$/n-c-Si heterointerface is 5% or less, so that there is no significant difference between both samples. Although the saturation of current density shown in Figs. 2(b) and 2(c) suggested the formation of oxide layers on the surface of p-$BaSi_2$ layer or heterointerface of p-$BaSi_2$/n-c-Si, these AES spectra show the formation of oxide layers on the surface of the p-$BaSi_2$ layer. Figure 4(c) show Ba/Si composition ratio in $BaSi_2$ thin films. In the depth range of 100 to 110 nm, where there is little influence of BaO and Si substrate on the Ba/Si composition ratio, the two-step sample has a composition closer to stoichiometry (Ba/Si = 0.5) compared with the one-step sample. The reason why Ba composition was reduced in the one-step sample is due to the diffusion of Ba into the Si substrate, since total amount of

deposited Ba is same. According to a previous report, a β-$FeSi_2$ seed layer is effective at preventing the diffusion of Fe into the Si substrate during $FeSi_2$ crystallization from Fe/Si multilayer stacks deposited on Si substrates [37]. Similarly, a stable $BaSi_2$ layer might be formed at the initial stage of deposition by the two-step method and thus the diffusion of Ba into Si substrate could be suppressed. Based on the results of AES measurements, we consider the cause of the observed difference in V_{oc}. For the one-step sample, p-$BaSi_2$ with non-stoichiometric composition was formed in the vicinity of the heterointerface, leading to a larger defect density and lower V_{oc}. On the other hand, in the case of the two-step sample, high V_{oc} could be achieved by forming p-$BaSi_2$ with nearly-stoichiometric composition since Ba atoms have sufficient time to diffuse toward the n-c-Si side. In addition, in the one-step sample, the p-$BaSi_2$ layer is Si-rich in comparison with the two-step sample, consequently impurities or defects tend to be generated in this layer. As a result, the R_s was increased and the J_{sc} was decreased.

Figure 5 shows the results of DLTS measurement. Since the carrier density in n-c-Si is much less than that in p-$BaSi_2$, it can be regarded that the signal originates from the n-c-Si side. Both the samples show the peak around 270 K. From this peak, defect densities in the two-step and one-step samples were estimated to be 1.5×10^{13} cm^{-3} and 1.2×10^{13} cm^{-3}, respectively [5]. Since the peaks are positive, these defects trapped minority carriers in the n-c-Si. Since the defect densities between one-step and two step samples are almost identical, the difference in V_{oc} is caused by the p-$BaSi_2$ side. One possible factor of decreasing V_{oc} is defect around interface due to their deposition rate of the first step.

From above these results, we attempted to optimize the solar cell structures by employing $BaSi_2$ prepared by the two-step method and back surface field layer (n^{++}-Si layer) to achieve high conversation efficiency, as show in Fig. 6(a). As a result, we obtained *J-V* characteristics shown in Fig. 6(b). V_{oc}=432 mV, J_{sc}=27.9 mA/cm^2, *FF*=50.8, and η=6.23 % were obtained. The *J-V* characteristics of the previous cell, which was fabricated by the one-step method, correspond to those of the "Light 3" shown in Fig. 2(b). All the parameters increase in comparison with previous one. Since J_{sc} and *FF* in the previous cell were influenced by the absence of ITO, the discussion about them is not necessary. The most remarkable thing is V_{oc}. In spite of a larger cell area of 1.44 cm^2 than a $BaSi_2$/Si heterojunction solar cell fabricated by a MBE method [28, 29], V_{oc} is shown to be comparable. If textured substrate

was used, higher conversation efficiency exceeding 10% can be attainable.

4. Conclusions

We have fabricated p-$BaSi_2$ film on n-c-Si(111) substrate by using thermal evaporation by one-step and two-step methods to clarify the effect of interface between c-Si and deposited p-$BaSi_2$ films. We confirmed that there is no significant difference between one-step and two-step samples in terms of FWHM of Raman spectra. AES measurement showed that the two-step sample is closer to stoichiometry in p-$BaSi_2$ layer. DLTS measurements indicated that the defect density around c-Si side of the one-step sample is almost same for the two-step sample. From *J-V* characteristics, V_{oc} was improved from 319 to 463 mV by the two-step method. The increase of built-in potential between the heterojunction led to improvement of V_{oc}. Finally, the conversion efficiency of 6.23%, V_{oc} of 432 mV, J_{sc} of 27.9 mA/cm^2, and *FF*=50.8% was achieved by optimized cell structure, suggesting that p-$BaSi_2$/n-c-Si heterojunction solar cells fabricated by thermal evaporation is promising to apply to large-area substrates.

Acknowledgments

This work was supported by the New Energy and Industrial Technology Development Organization (NEDO) and JSPS KAKENHI Grant Number 20H05187. The authors thank M. F. Hainey Jr. from Nagoya University for his help with English correction.

References

1) G. Niu, X. Guo and L. Wang, J. Matter. Chem. A, **3** 8970 (2015).
2) T. M. Friedlmeier, P. Jackson, A. Bauer, D. Hariskos, O. Kiowski, R. Menner, R. Wuerz and M. Powalla, Thin Solid Films **633**, 13 (2017).
3) M. Gloeckler, I. Sankin and Z. Zhao, IEEE J. Photovol. **3**, 4 (2013).
4) K. Morita, Y. Inomata, and T. Suemasu, Thin Solid Films **508**, 363 (2006).
5) H. Takeuchi, W. Du, M. Baba, R. Takabe, K. Toko and T. Suemasu, Jpn. Appl. Phys. **54**, 07JE01 (2015).
6) W. Du, M. Baba, K. Toko, K. O. Hara, K. Watanabe, T. Sekiguchi, N. Usami, and T. Suemasu, J. Appl. Phys. **115**, 223701 (2014)

7) K. Toh, T. Saito and T. Suemasu, Jpn. J. Appl. Phys. **50**, 068001 (2011).
8) T. Suemasu, K. Morita, M. Kobayshi, M. Saida and M. Sasaki, Jpn. J. Appl. Phys. **45**, L519 (2006).
9) K. O. Hara, N. Usami, K. Toh, M. Baba, K. Toko and T. Suemasu, J. Appl. Phys. **112** 083108 (2012).
10) K. O. Hara, N. Usami, K. Nakamura, R. Takabe, M. Baba, K. Toko and T. Suemasu, Appl. Phys. Express **6**, 112302 (2013).
11) R. Takabe, K. O. Hara, M. Baba, W. Du, N. Shimada, K. Toh, N. Usami and T. Suemasu, J. Appl. Phys. **115**, 193510 (2014).
12) M. Baba, K. Toh, K. Toko, N. Saito, N. Yoshizawa, K. Jipther, T. Sakiguchi, K. O. Hara, N. Usami and T. Suemasu, J. Cryst. Growth **348**, 75 (2012).
13) M. Baba, K. Watanabe, K. O. Hara, K. Toko, T. Sekiguchi, N. Usami and T. Suemasu, Jpn. J. Appl. Phys. **53**, 078004 (2014).
14) D. B. Migas, V. L. Shaposhnikov and V. E. Borisenko, Phys. Status Solidi B **224**, 2611 (2007).
15) K. Toh, T. Saito and T. Suemasu, Jpn. J. Appl. Phys. **50**, 068001 (2014).
16) M. Kumar, N. Umezawa and M. Imai, J. Appl. Phys. **115**, 203718 (2014).
17) T. Suemasu, Jpn. J. Appl. Phys. **54**, 07JA01 (2015).
18) K. O. Hara, Y. Nakagawa, T. Suemasu and N. Usami, Jpn. J. Appl. Phys. **54**, 07JE02 (2015).
19) Y. Nakagawa, K. O. Hara, T. Suemasu and N. Usami, Jpn. J. Appl. Phys. **54**, 08KC03 (2015).
20) K. O. Hara, J. Yamanaka, K. Arimoto, K. Nakagawa, T. Suemasu and N. Usami, Thin Solid Films **595**, 68 (2015).
21) K. O. Hara, Y. Nakagawa, T. Suemasu and N. Usami, Procedia Eng. **141**, 27 (2016).
22) Y. Nakagawa, K. O. Hara, T. Suemasu and N. Usami, Procedia Eng. **141**, 23 (2016).
23) K. O. Hara, C. T. Trinh, K. Arimoto, J. Yamanaka, K. Nakagawa, Y. Kurokawa, T. Suemasu, N. Usami, J. Appl. Phys. **120**,045103 (2016).
24) K. O. Hara, K. Arimoto, J. Yamanaka and K. Nakagawa, J. Mater. Res. **33**, 16, 2297 (2018).
25) N. M. Shaalan, K. O. Hara, C. T. Trinh, Y. Nakagawa and N. Usami, Mater. Sci. Semicond. Process. **76**, 37 (2018)
26) C. T. Trinh, Y. Nakagawa, K. O. Hara, R. Takabe, T. Suemasu and N. Usami, Mater. Res.

Express 3, 7, 076204 (2016).

27) D. Tsukahara, S. Yachi, H. Takeuchi, R. Takabe, W. Du, M. Baba, Y. Li, K. Toko, N. Usami and T. Suemasu, Appl. Phys. Lett. **108**, 152101 (2016).

28) S. Yachi, R. Takabe, H. Takeuchi, K. Toko, T. Suemasu, Appl. Phys. Lett. **109,** 072103 (2016)

29) T. Deng, T. Sato, Z. Xu, R. Takabe, S. Yachi, Y. Yamashita, K. Toko and T. Suemasu, Appl. Phys. Express **11**, 062301 (2018).

30) K. Takahashi, Y. Nakagawa, K. O. Hara, I. Takahashi, Y. Kurokawa and N. Usami, MRS Advances **3**, 25, 1435 (2018).

31) K. O. Hara, C. Yamamoto, J. Yamanaka, K. Arimoto, K. Nakagawa, and N. Usami, Jpn. J. Appl. Phys. **57**, 04FS01 (2018).

32) K. O. Hara, N. Usami, Y. Hoshi, Y. Shiraki, M. Suzuno, K. Toko, and T. Suemasu, Jpn. J. Appl. Phys. **50**, 121202, (2011).

33) R. Varache, C. Leendertz, M. E. Gueunier-Farret, J. Haschke, D. Muñoz and L. Korte, Sol. Energy Mater. Sol. Cells **141** 14, (2015).

34) K. Y. Tsou, and E. B. Hensley, J. Appl. Phys. **45**, 47, (1974).

35) H. Hoshida, T. Suemasu, and Y. Terai, Defect Diffus. Forum **386**, 43 (2018).

36) M. Diem, Modern Vibrational Spectroscopy and Micro-Spectroscopy, 1st ed. (John Wiley & Sons, Chichester, 2015), Chap. 4.2.

37) T. Suemasu, N. Hiroi, T. Fujii, K. Takahara and F. Hasegawa, Jpn. J. Appl. Phys. **38**, 8A (1999).

Figure Captions

Fig. 1. Current profiles of (a) one-step and (b) two-step method in the W boat during thermal evaporation.

Fig. 2. (a) Schematics of $BaSi_2$/c-Si heterojunction solar cells. Dark and illuminated *J-V* characteristics of the sample fabricated by (b) one-step and (c) two-step methods. (d) Calculated band diagram of the p-$BaSi_2$/BaO/n-c-Si structure. The band diagram was calculated by a one-dimensional device simulator, Afors-HET ver 2.5 [33].

Fig. 3. Raman scattering spectra of the films prepared by one-step and two-step methods.

Fig. 4. Depth profile of Ba, Si, and O atomic composition of a part of area in the films prepared by (a) the one-step and (b) two-step methods. The region where the Si composition is above 80% was regarded as a c-Si. The region where the sum of Ba and Si composition is above 80% was regarded as $BaSi_2$. The region where Ba exists and O composition is above 20% was regarded as BaO. (c) Ba/Si composition ratio in the range of $BaSi_2$ thin films. The dashed line shows a stoichiometric composition of $BaSi_2$.

Fig. 5. DLTS spectra of the samples prepared by (a) one-step and (b) two-step methods.

Fig. 6. (a) Schematics of optimized solar cell structure. (b) Illuminated *J-V* characteristics before and after optimization.

Table I. J_{sc}, V_{oc}, FF and η value for the solar cells fabricated by one-step and two-step methods. The structure of solar cells is shown in Fig. 2(a).

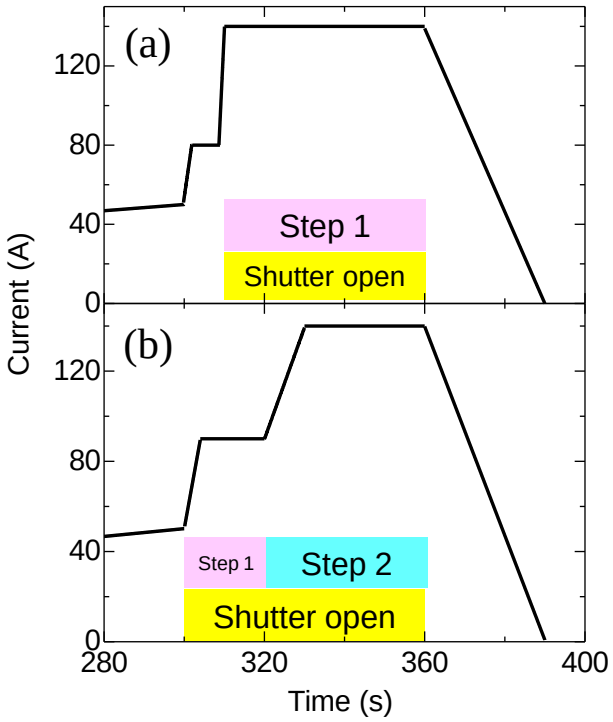

Fig. 1. (Color online)

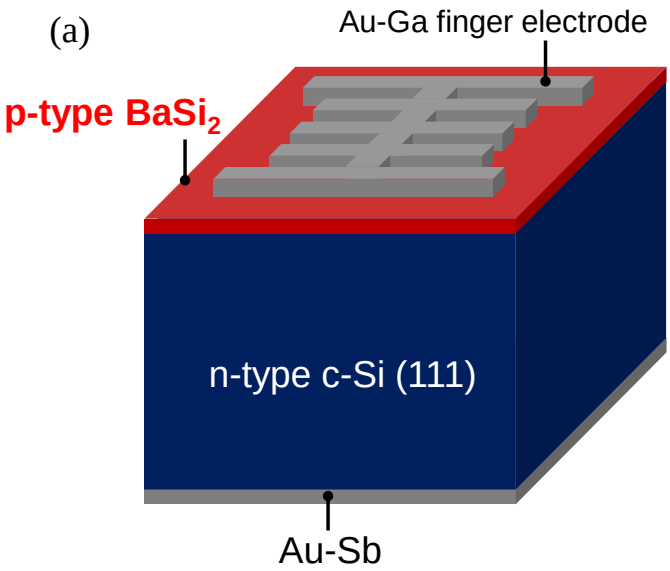

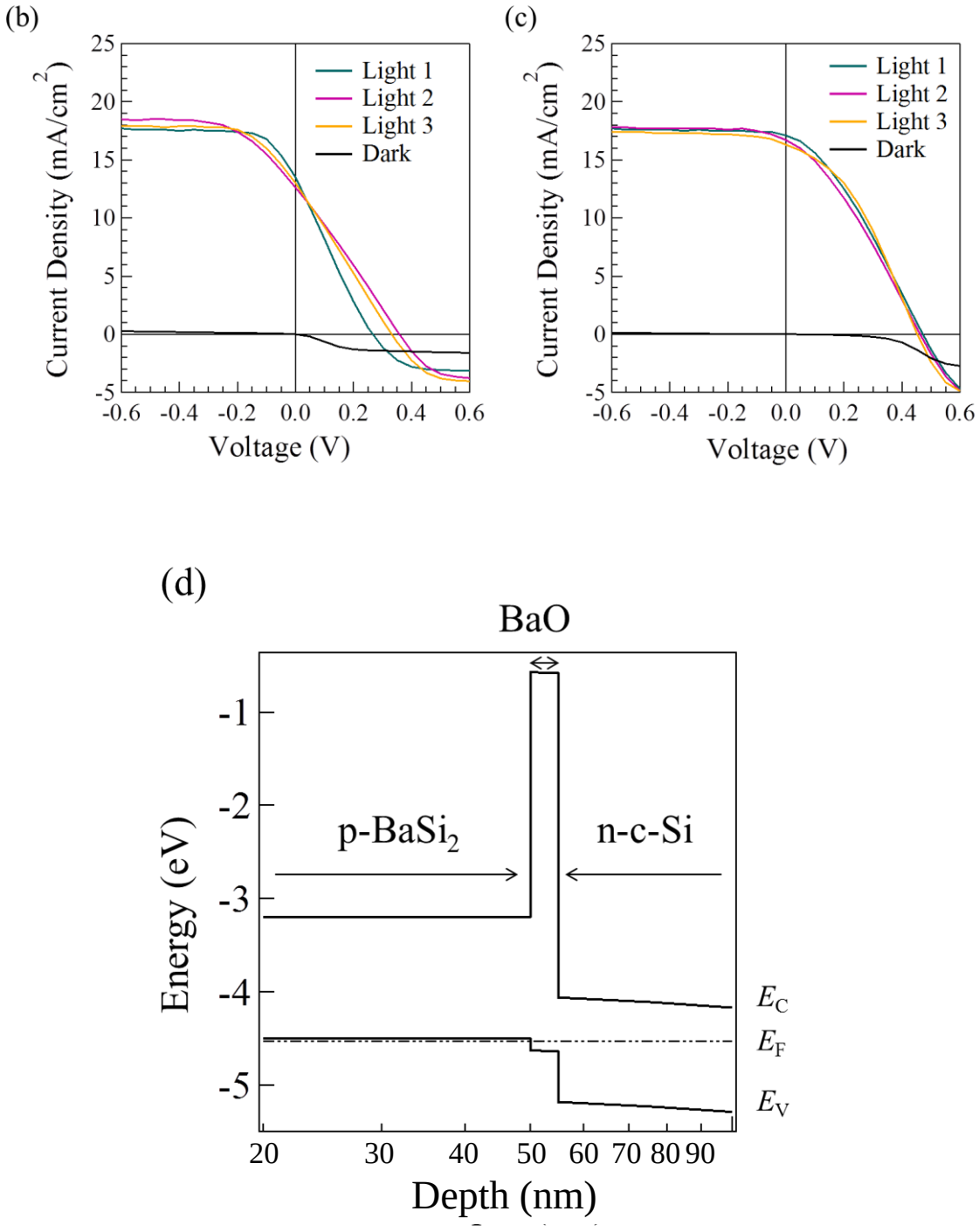

Fig. 2. (Color online)

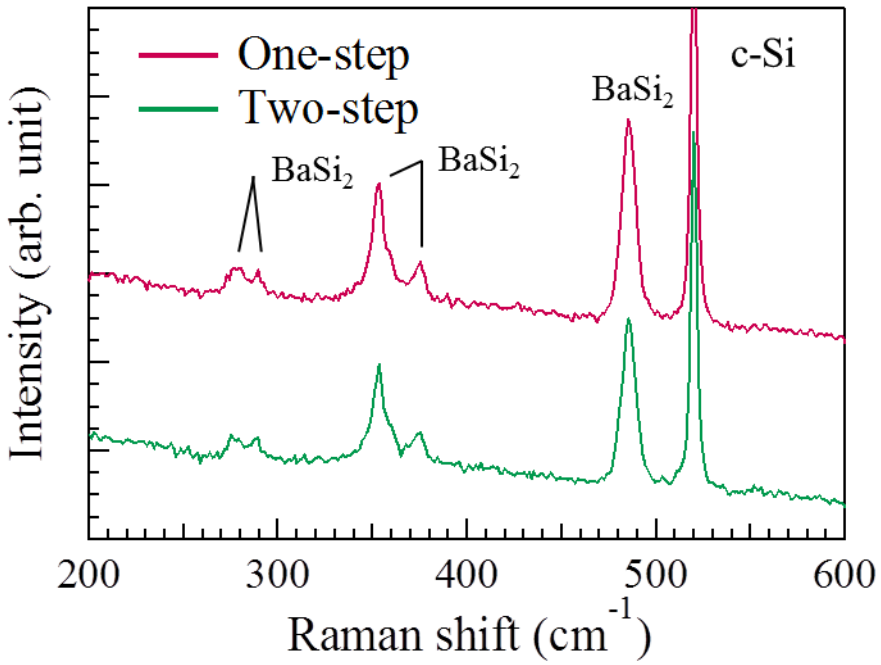

Fig. 3. (Color online)

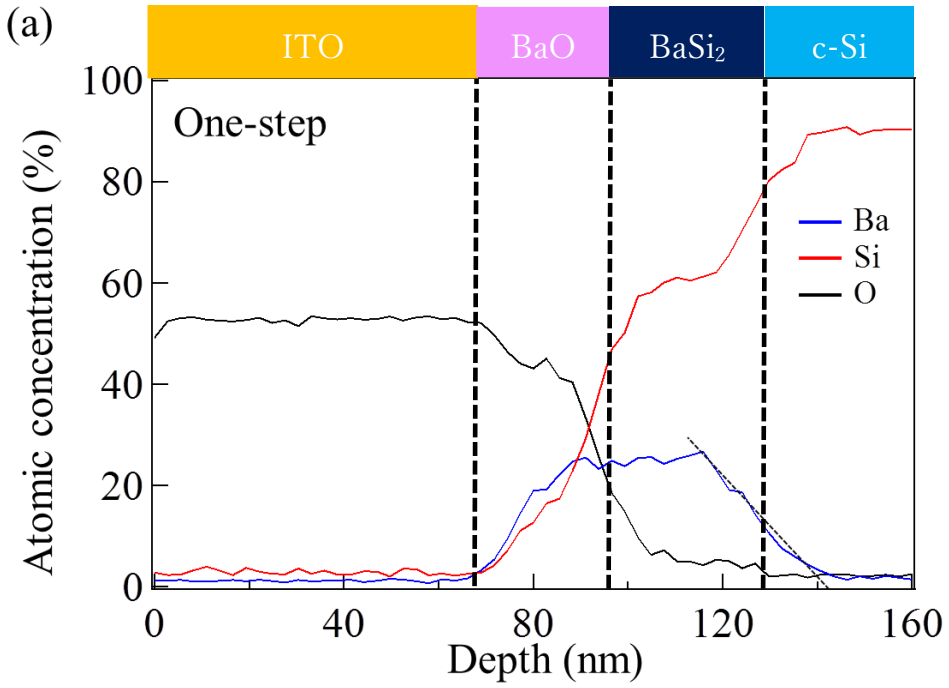

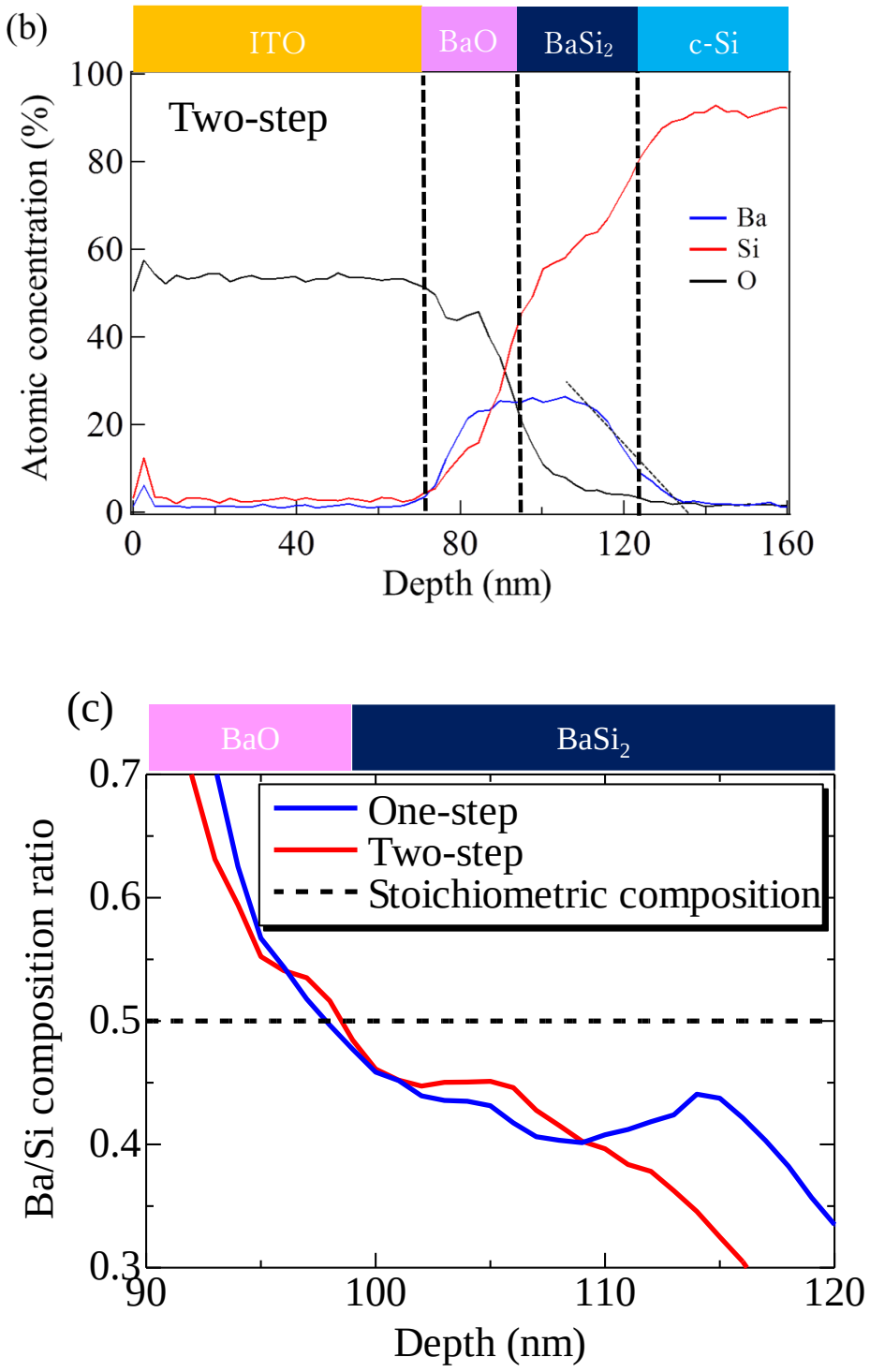

Fig. 4. (Color online)

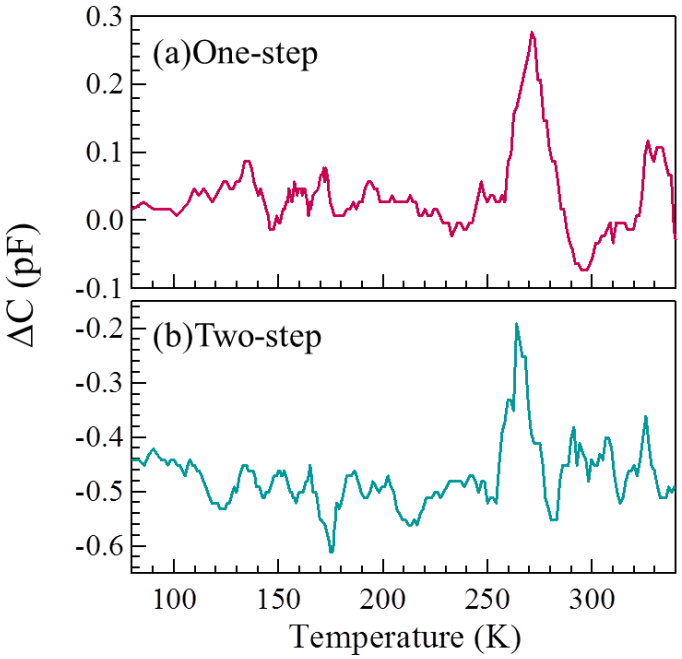

Fig. 5. (Color online)

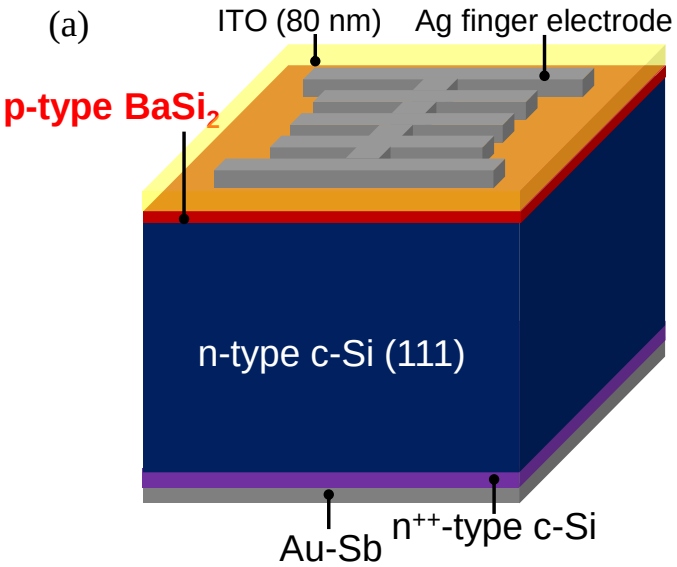

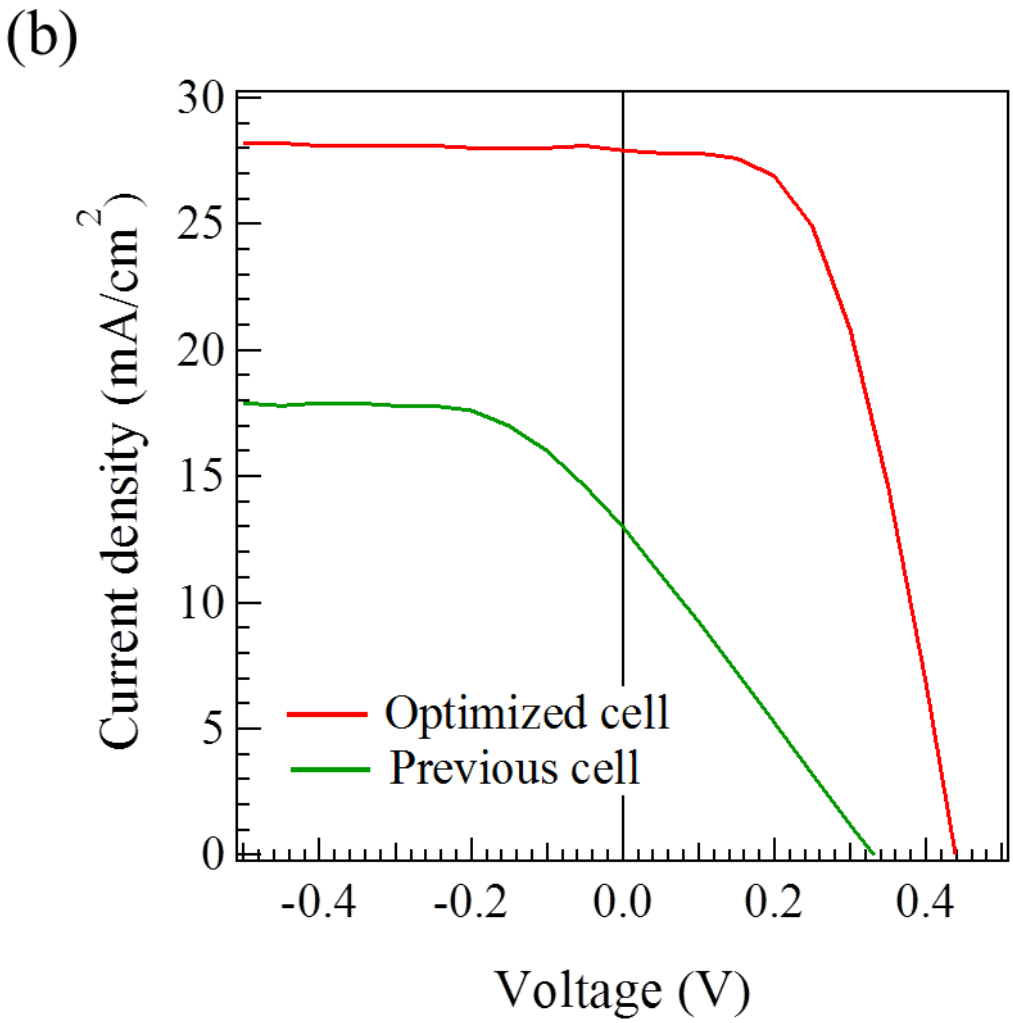

Fig. 6. (Color online)

Table I

Method	J_{sc} (mA/cm^2)	V_{oc} (mV)	FF(%)	η (%)
One-step	13.0	319	25	1.03
Two-step	16.7	463	34	2.63